Synthesis of Macrocyclic Copolymer Brushes and Their Self-Assembly into Supramolecular Tubes

Michel Schappacher, *et al.*

Science **319**, 1512 (2008);
DOI: 10.1126/science.1153848

Science (print ISSN 0036-8075; online ISSN 1095-9203) is published weekly, except the last week in December, by the American Association for the Advancement of Science, 1200 New York Avenue NW, Washington, DC 20005.

density waves in simple metals have been unsuccessful, it is conceivable that fluctuations characteristic of such states dynamically enhance the nesting properties of the Fermi surface and hence the propensity for Kohn anomalies in the phonon spectrum. Indeed, experiments on charge-density-wave materials such as $NbSe_2$ have revealed Kohn anomalies (*8*) and Fermi-surface “pseudogaps” (*24*, *25*) in the extended fluctuation regime at temperatures well above the onset of static density-wave order. Detailed theoretical work is required to assess whether interference between density-wave and superconducting correlations can limit the growth of the superconducting gap and lead to the observed convergence of both energy scales at low temperatures.

Our experiments on two different elemental superconductors demonstrate that the low-temperature limit of the superconducting energy gap coincides with low-lying Kohn anomalies in transverse acoustic phonons. Because both superconductors exhibit different lattice structures, phonon spectra, Fermi surfaces, and superconducting gaps, this coincidence cannot be accidental. Although its origin is presently unclear, a specific scenario to explore in future theoretical work is the interplay between density-wave and superconducting correlations. Lastly, we point out a possible analogy to research on high-temperature superconductors, where an anomalous coincidence of the superconducting gap with a weakly temperature-dependent pseudogap has recently been reported in some regions of momentum space (*26*–*28*).

References and Notes

1. J. Bardeen, L. N. Cooper, J. R. Schrieffer, *Phys. Rev.* **108**, 1175 (1957).
2. For a review, see J. R. Schrieffer, *Theory of Superconductivity* (Perseus, New York, 1999).
3. For recent advances in ab initio computation of superconducting properties, see M. A. L. Marques *et al.*, *Phys. Rev. B* **72**, 024546 (2005).
4. W. Kohn, *Phys. Rev. Lett.* **2**, 393 (1959).
5. B. N. Brockhouse, T. Arase, G. Caglioti, A. D. B. Woods, *Phys. Rev.* **128**, 1099 (1962).
6. R. Stedman, L. Almquist, G. Nilsson, G. Raunio, *Phys. Rev.* **163**, 567 (1967).
7. Y. Nakagawa, A. D. B. Woods, *Phys. Rev. Lett.* **11**, 271 (1963).
8. D. E. Moncton, J. D. Axe, F. J. DiSalvo, *Phys. Rev. B* **16**, 801 (1977).
9. S. M. Shapiro, G. Shirane, J. D. Axe, *Phys. Rev. B* **12**, 4899 (1975).
10. S. P. Bayrakci, T. Keller, K. Habicht, B. Keimer, *Science* **312**, 1926 (2006).
11. T. Keller *et al.*, *Phys. Rev. Lett.* **96**, 225501 (2006).
12. T. Keller *et al.*, *Appl. Phys. A* **74**, S332 (2002).
13. Materials and methods are available on *Science* Online.
14. J. R. Anderson, A. V. Gould, *Phys. Rev.* **139**, A1459 (1963).
15. H. J. Maris, W. E. Massey, *Phys. Rev. Lett.* **25**, 220 (1970).
16. L. P. Pitayevski, Y. B. Levinson, *Phys. Rev. B* **14**, 263 (1976).
17. R. F. Gasparovic, B. N. Taylor, R. K. Eck, *Solid State Commun.* **4**, 59 (1966).
18. M. A. Moore, D. I. Paul, *Solid State Commun.* **9**, 1303 (1971).
19. P. B. Allen, *Phys. Rev. B* **6**, 2577 (1972).
20. S. Pisana *et al.*, *Nat. Mat.* **6**, 198 (2007).
21. E. Cappelluti, *Phys. Rev. B* **73**, 140505 (2006).
22. O. V. Dolgov, O. K. Andersen, I. I. Mazin, *Phys. Rev. B* **77**, 014517 (2008).
23. A. W. Overhauser, *Phys. Rev.* **128**, 1437 (1962).
24. S. V. Borisenko *et al.*, preprint available at www.arXiv.org/abs/0704.1544.
25. T. Kiss *et al.*, *Nat. Phys.* **3**, 721 (2007).
26. K. Tanaka *et al.*, *Science* **314**, 1910 (2006); published online 15 November 2006 (10.1126/science.1133411).
27. K. Terashima *et al.*, *Phys. Rev. Lett.* **99**, 017003 (2007).
28. W. S. Lee *et al.*, *Nature* **450**, 81 (2007).
29. D. L. Waldorf, *Bull. Am. Phys. Soc.* **5**, 170 (1960).
30. R. C. Dynes, V. Narayanamurti, J. P. Garno, *Phys. Rev. Lett.* **41**, 1509 (1978).
31. We thank O. K. Andersen, S. P. Bayrakci, S. V. Borisenko, M. Cardona, O. Dolgov, E. K. U. Gross, and G. Khaliullin for fruitful discussions; C. T. Lin for the Pb crystals; J. Mayor for the Nb crystals; and K. Buchner for technical assistance.

Supporting Online Material

www.sciencemag.org/cgi/content/full/1154115/DC1
Materials and Methods
Fig. S1
References and Notes

13 December 2007; accepted 1 February 2008
Published online 21 February 2008;
10.1126/science.1154115
Include this information when citing this paper.

Synthesis of Macrocyclic Copolymer Brushes and Their Self-Assembly into Supramolecular Tubes

Michel Schappacher and Alain Deffieux*

We report on an efficient route to design large macrocyclic polymers of controlled molar mass and narrow dispersity. The strategy is based on the synthesis of a triblock copolymer A**B**C, in which the long central block **B** is extended by two short A and C sequences bearing reactive antagonist functions. When reacted under highly dilute conditions, this precursor produces the corresponding macrocycle by intramolecular coupling of the A and C blocks. Chloroethyl vinyl ether was selected as the monomer for the central block **B**, because it can be readily derivatized into brushlike polymers by a grafting process. The corresponding macrocyclic brushes were decorated with polystyrene or randomly distributed polystyrene and polyisoprene branches. In a selective solvent for the polyisoprene branches, the macrocyclic brushes self-assemble into cylindrical tubes of up to 700 nanometers.

The interest in cyclic macromolecules began more than 50 years ago with the theoretical prediction of the effect of chain cyclization on polymer properties (*1*, *2*) and the discovery of naturally occurring macrocycles such as DNA (*3*). Recently, the self-assembly of proteins into nanorings for the fabrication of advanced materials has been reported (*4*). Because of their very limited availability, large polymer macrocycles remain a fascinating curiosity for theoreticians and physicists and a challenging area for synthetic chemists (*5*).

Macrocyclic polymers were first obtained from macromolecules systems exhibiting ring-linear chain equilibria (*6*). In such systems, low-to-medium molar mass macrocycles are obtained generally in admixture with linear chains, although a more selective approach has been recently reported by Grubbs (*7*).

The most appropriate method for the synthesis of cyclic polymers with controlled size and narrow dispersity was first proposed by Casassa (*8*) more than 40 years ago. It is based on the end-to-end chain coupling of linear α,ω-difunctional chains in highly dilute conditions. Coupling of α,ω-dianionic polymers with difunctional agents has been the most extensively used ring closure approach (*9*–*11*); however, cyclization yields for large macrocycles are generally low, and fractionation procedures are required to remove residual linear chains and polycondensates (*12*). An alternative route is based on the end-to-end coupling of α,ω-heterodifunctional linear chain (*13*). Cyclization is performed under high dilution by selective activation of one polymer end, which reacts intramolecularly with the second chain end. Higher cyclization yields have been reported but molar masses of the macrocycles remain limited. A more selective approach was proposed by Tezuka (*14*) that involves the precyclization of linear chains bearing ionic end groups. However, only very low molar mass macrocycles have been synthesized.

The preparation of large macrocyclic polymers and copolymers is thus limited (*12*) by (i) the difficulty to get pure α,ω-difunctional high molar mass precursors, (ii) the drastic decrease of the end-to-end ring closing efficiency when in-

---

CNRS, Université Bordeaux 1, Ecole Nationale Supérieure de Chimie et Physique de Bordeaux (ENSCPB), Laboratoire de Chimie des Polymères Organiques, Unité Mixte de Recherche 5629, 16 Avenue Pey Berland, 33607 Pessac cedex, France.

*To whom correspondence should be addressed. E-mail: deffieux@enscpb.fr

creasing the distance between chain ends, and (iii) the problem of elimination of linear contaminants of the same high molar mass.

We have developed a method to synthesize large polymer macrocycles based on the synthesis of an A**B**C triblock copolymer, in which the long central **B** block is extended by two short A and C sequences bearing monomer units with reactive antagonist functions (Fig. 1). The external blocks are then selectively activated under dilute conditions to allow intramolecular coupling between the A and C blocks and form the macrocyclic polymers, with further functionalization to form the corresponding brush polymers with polystyrene (PS) or randomly distributed polystyrene and polyisoprene (PS/PI) branches.

The A**B**C copolymers were obtained by sequential living cationic polymerization of three different vinyl ethers (fig. S1). The short A block consists of units of *ter*-butyl dimethyl silyl ethoxy vinyl ether (a hydroxy-protected vinyl ether). Chloroethyl vinyl ether (CEVE) was selected as the second monomer for the **B** block, because PCEVE [poly(CEVE)] can be readily converted into the corresponding PS brush structure (*15*). Finally, block C was grown by addition of cyclohexane dimethanol divinyl ether (a divinyl ether), which allows introducing monomer units bearing vinyl ether side groups in appropriate reaction conditions. Detailed information on the synthesis methods can be found in the supporting online material.

Typically, the triblock copolymers were constituted to A, **B**, and C blocks with targeted average degree of polymerization ($\overline{\mathrm{DP}}_n$) of roughly 5, 1000, and 5, respectively. The properties of the A**B**C copolymer "(L)" are given in Table 1.

After deprotection of the hydroxyls on the block A's, cyclization was achieved under high dilution via their intramolecular reaction with the vinyl ether functions on block C's in the presence of an acid salt as a catalyst. The size exclusion chromatograms (SECs) of the A**B**C copolymer before and after cyclization are shown in Fig. 2.

The shift of the main SEC peak to higher elution volume is consistent with the reduction of the hydrodynamic volume of the macromolecule after chain cyclization (*16*). The slight peak broadening and the presence of two small peak shoulders indicate the presence of a limited amount of residual linear precursor and of linear or cyclic dimers. Some characteristics of cyclic copolymer "(C)" that formed are indicated in Table 1. It is difficult to get more precise and direct information on the architecture of the polymers formed and on the cyclization yield, with conventional analytical techniques.

The synthesis of PS brushes by grafting living polystyryl lithium (PSLi) and/or polyisoprenyl lithium (PILi) onto PCEVE chains has been studied in our group (*17*, *18*). One advantage of this approach relies on the capacity to precisely control the architecture and dimensions of the brush, given that both the PCEVE backbone and the PS grafts are obtained by living polymerizations. In addition, the good efficiency and selectivity of the coupling reaction allow the preparation of brush polymers exhibiting the same architecture as the initial PCEVE backbone as shown by atomic force microscopy (AFM) (*19*). This strategy was applied here to convert large macrocyclic polymers into the corresponding cyclic PS brushes. This approach had been tried with cyclic PCEVE of low molar mass prepared from an α,ω-heterodifunctional precursor (*20*), but the formation of cyclic brush was not demonstrated.

The SEC chromatogram of a cyclic *brush*-Ca is shown in Fig. 2. The main elution peak can be attributed to macrocyclic brushes, whereas the two small shoulders observed at lower elution volume have been assigned on the basis of static light scattering (SLS) measurements (*21*) to linear PS brushes and to brush dimers of various architec-

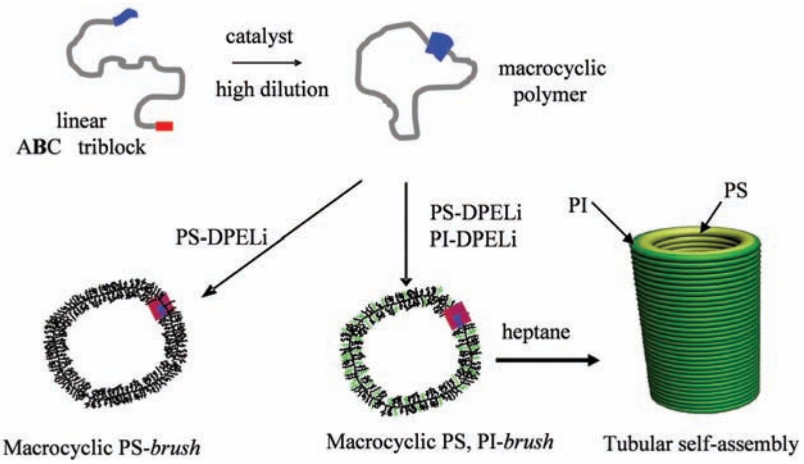

Fig. 1. Strategy for the synthesis of cyclic comblike copolymers and their self-assembly. PS-DPELi, (1,1-diphenylethylene) end-capped polystyryllithium; PI-DPELi, (1,1-diphenylethylene) end-capped polyisoprenyllithium.

Table 1. Dimensional characteristics of linear (L) and cyclized (C) A**B**C copolymer and of the corresponding macrocyclic brushes with different PS or PS/PI branch lengths. M_n, number-average molecular weight; M_w, weight-average molecular weight; M_n *app*, apparent M_n; M_p *app*, apparent SEC peak molecular weight.

Chain architecture*	$\overline{\mathrm{DP}}_n$†	M_n *app*‡ (× 10^{-3})	M_w/M_n	M_p *app*‡ (× 10^{-3})	M_w§ (× 10^{-3})
L	0	92	1.05	99	95
C	0	78	1.15	76	96
PS *brush*-Ca	90/0	740	1.14	800	5900
PS *brush*-Cb	260/0	1650	1.09	2160	10,200
PS/PI *brush*-Cc‖	170/50	872	1.10	967	6800

*$\overline{DP}_n$ of PCEVE is 870. †$\overline{DP}_n$ of PS or PI branches. ‡Determined by SEC in THF by means of PS standards. §Measured by SLS with refractive index increments (*dn/dc*) of 0.09 (PCEVE L and C), 0.18 (PS brushes), and 0.15 (PS/PI *brush*). ‖Number of PS and PI branches per macromolecule are 400 and 350, respectively, which corresponds to 80% in weight of PS.

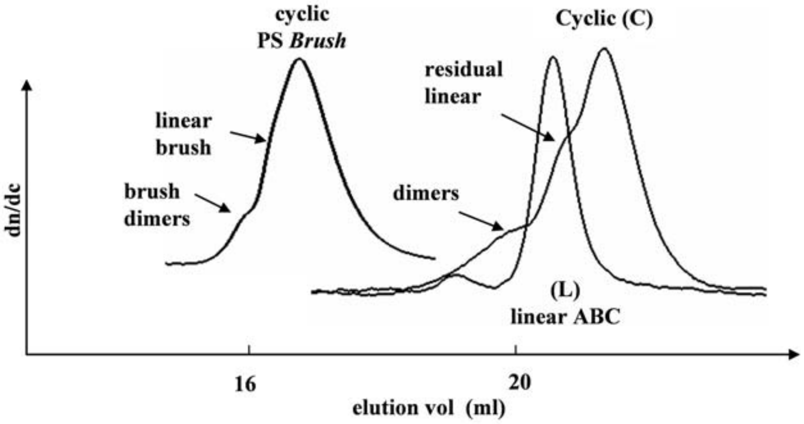

Fig. 2. SECs in tetrahydrofuran (THF) of A**B**C copolymer (L), cyclized polymer (C), and corresponding cyclic PS *brush*-Ca (see Table 1).

tures. Direct imaging (*19*, *22–24*) allowed us to confirm these conclusions and to get direct and quantitative information on the cyclic polymer structures obtained. The AFM topographic image of *brush*-Ca (Fig. 3A) shows single macromolecules isolated on the highly oriented pyrolytic graphite surface. Most of the structures observed are monodispered macrocyclic brushes, which agrees with a cyclization efficiency of 50 to 60%. Among the other polymer architectures observed are linear brushes corresponding to uncyclized A**B**C copolymer, linear and macrocyclic dimers exhibiting about twice the size of the linear precursor or of the corresponding cyclics, and tadpole structures.

Samples containing larger fractions of macrocyclic brushes were readily obtained by selective precipitation from cyclohexane solution upon gradually decreasing the temperature from 19° to 18°C, corresponding to the theta conditions of comb PS. The AFM image of the fractionated *brush*-Ca is shown in Fig. 3B. Typically, the fractionated samples contain about 80 to 85% of cyclic brushes. The main characteristics of the cyclic brushes are provided in Table 1. The influence of the PS graft dimensions on the characteristics of the brush macrocycles is shown in Fig. 3, C and D, for samples with ($\overline{DP}_n$) of 90 and 260, respectively. The two cyclic brushes obtained from a PCEVE with a $\overline{DP}_n$ of 870 are characterized by a mean average diameter of 65 to 70 nm for the central backbone (fig. S2). This yields a circumference of 205 to 220 nm for the cyclized PCEVE. Assuming a $\overline{DP}_n$ of 870 and a value of 2.5 Å per monomer unit, this corresponds to a fully extended backbone conformation (870 nm × 0.25 nm = 217.5 nm). This can be explained by the steric hindrance and compactness near the PCEVE backbone resulting from the high PS grafting density, which according to the brush molar mass (Table 1) corresponds to about three PS grafts every four CEVE units. However, no chain breaking was observed despite the strong mechanical forces applied to the PCEVE backbone. The crown section and the size of the central cavity are determined by the branch length and can be tuned by controlling the PS $\overline{DP}_n$. As it may be seen (Fig. 3, A and D), the macrocycles as well as other brush architectures are separated by an almost constant distance, which corresponds to the length of two PS branches in an almost fully extended conformation (fig. S2).

To obtain the corresponding cyclic copolymer brushes with PS/PI branches, we successively reacted polystyryllithium and polyisoprenyllithium both end-capped with 1,1-diphenylethylene in determined amounts with the macrocyclic PCEVE to yield cyclic brushes with PS/PI branches that were randomly distributed (Fig. 1). The characteristics of one cyclic PS/PI brush used in this study are indicated in Table 1. Its capacity to self-organize was investigated in heptane—a selective solvent of the PI blocks—by dynamic light scattering (DLS) and by AFM as solid deposits from their solutions. In heptane, the cyclic PS/PI brush copolymer self-assembles, forming a single and monodisperse population of large cylindrical objects with an average hydrodynamic radius of 200 nm. The corresponding DLS data are available as supporting online material (fig. S3). Further insight in these supramolecular structures was gained by AFM analysis (Fig. 3, E and F). The selective formation of rigid tubular objects (with section diameters of about 100 nm, corresponding to elementary macrocyclic PS/PI brushes, and lengths of up to 700 nm) that were either isolated or aggregated is observed. This agrees with the self-assembly of elementary cyclic brushes directed by intermolecular association between PS branches, whereas the PI grafts ensure their dispersion/solubilization into the selective PI solvent. Although they are not observed in heptane solution, the formation of clusters of tubular objects observed on AFM images (Fig. 3E) likely takes place during solvent evaporation on graphite. The length of the supramolecular tubes, as well as the observed structural defects, results from the contribution of remaining linear and other brush structures that perturb or stop the self-assembly of brush macrocycles.

We have developed a selective route to large macrocylic polymers based on the coupling of external short blocks of A**B**C-type copolymers. The substantial increase in cyclization efficiency can be attributed both to the high functionality of ABC precursor and to the presence of several reactive functions at each chain end that increase the probability of intramolecular end-to-end cyclization. As indicated by the absence of cross-linked chains or high polycondensates, the presence of several reactive groups at each chain end does not yield significant multichain coupling under high dilution.

The obtained macrocyclic brushes constitute a class of macromolecules with a precise and tunable chain architecture that can be used as such or as elementary building blocks for the preparation of supramolecular tubes, the structure of which can be eventually frozen by cross-linking. By changing the character and proportion of the constitutive blocks, tubular assemblies are expected

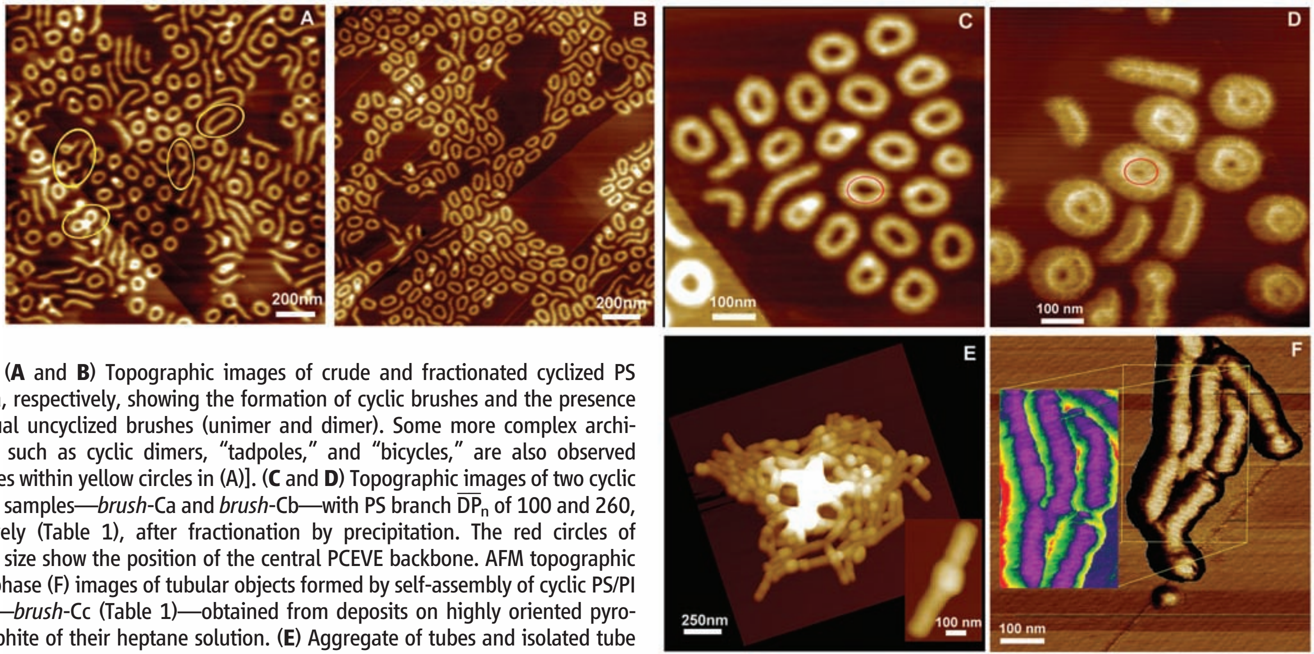

Fig. 3. (**A** and **B**) Topographic images of crude and fractionated cyclized PS *brush*-Ca, respectively, showing the formation of cyclic brushes and the presence of residual uncyclized brushes (unimer and dimer). Some more complex architectures, such as cyclic dimers, "tadpoles," and "bicycles," are also observed [structures within yellow circles in (A)]. (**C** and **D**) Topographic images of two cyclic PS brush samples—*brush*-Ca and *brush*-Cb—with PS branch $\overline{DP}_n$ of 100 and 260, respectively (Table 1), after fractionation by precipitation. The red circles of identical size show the position of the central PCEVE backbone. AFM topographic (E) and phase (F) images of tubular objects formed by self-assembly of cyclic PS/PI brushes—*brush*-Cc (Table 1)—obtained from deposits on highly oriented pyrolytic graphite of their heptane solution. (**E**) Aggregate of tubes and isolated tube (diameter, 100 nm; length, 600 nm). (**F**) Series of tubes interconnected by their polyisoprene shell (black) and image in reverse mode showing the internal PS (purple) and external PI (green) parts. The stripes corresponding to the elementary macrocyclic copolymer brushes are also visible.

to be formed in different media, whereas the inner surface of the tube can be tuned for a targeted application by selecting a second type of constitutive block of appropriate characteristics and properties.

References and Notes

1. B. H. Zimm, W. H. Stockmayer, *J. Chem. Phys.* **17**, 1301 (1949).
2. V. Bloomfield, B. H. Zimm, *J. Chem. Phys.* **44**, 315 (1966).
3. R. Dulbecco, M. Vogt, *Proc. Natl. Acad. Sci. U.S.A.* **50**, 236 (1963).
4. J. C. T. Carlson *et al.*, *J. Am. Chem. Soc.* **128**, 7630 (2006).
5. A. Deffieux, R. Borsali, in *Macromolecular Engineering: Precise Synthesis, Materials Properties, Applications*, K. Matyjaszewski, Y. Gnanou, L. Leibler, Eds. (Wiley-VCH, Weinheim, Germany, vol. 2, 2007), pp. 875–908.
6. J. A. Semlyen, G. R. Walker, *Polymer* **10**, 597 (1969).
7. C. W. Bielawski, D. Benitz, R. H. Grubbs, *Science* **297**, 2041 (2002).
8. E. F. Cassassa, *J. Polym. Sci. A* **3**, 605 (1965).
9. B. Vollmert, J. X. Huang, *Makromol. Chem. Rapid Commun.* **2**, 467 (1981).
10. G. Hild, C. Strazielle, P. Rempp, *Eur. Polym. J.* **19**, 721 (1983).
11. J. Roovers, P. Toporowski, *Macromolecules* **16**, 843 (1983).
12. T. E. Hogen-Esch, *J. Polym. Sci. Polym. Chem.* **44**, 2139 (2006).
13. M. Schappacher, A. Deffieux, *Makromol. Chem. Rapid Commun.* **12**, 447 (1991).
14. Y. Tezuka, H. Oike, *J. Am. Chem. Soc.* **123**, 11570 (2001).
15. A. Deffieux, M. Schappacher, *Macromolecules* **32**, 1797 (1999).
16. G. Hadziioannou *et al.*, *Macromolecules* **20**, 493 (1987).
17. M. Schappacher, A. Deffieux, *Macromolecules* **33**, 7371 (2000).
18. M. Schappacher, Z. Muchtar, A. Deffieux, *Macromolecules* **34**, 7595 (2001).
19. P. Viville *et al.*, *Polymer* **45**, 1833 (2004).
20. M. Schappacher, C. Billaud, C. Paulo, A. Deffieux, *Macromol. Chem. Phys.* **200**, 2377 (1999).
21. Assignment of peaks and peak shoulders on the SEC of polymer brushes to dimer, linear, and cyclic structures (Fig. 2) was made on the basis of their radius of gyration measured by SLS with a online laser light scattering detector.
22. M. Schappacher, A. Deffieux, *Macromolecules* **38**, 4942 (2005).
23. S. S. Sheiko, M. Möller, *Chem. Rev.* **101**, 4099 (2001).
24. S. S. Sheiko, in *Advances in Polymer Science: New Developments in Polymer Analytics II* (Springer Berlin, Heidelberg, vol. 151, 2000), pp. 61–174.

Supporting Online Material

www.sciencemag.org/cgi/content/full/319/5869/1512/DC1
Materials and Methods
Figs. S1 to S3
References

6 December 2007; accepted 1 February 2008
10.1126/science.1153848

Splitting of the 520-Kilometer Seismic Discontinuity and Chemical Heterogeneity in the Mantle

Ashima Saikia,* Daniel J. Frost, David. C. Rubie

Seismic studies indicate that beneath some regions the 520-kilometer seismic discontinuity in Earth's mantle splits into two separate discontinuities (at ~500 kilometers and ~560 kilometers). The discontinuity near 500 kilometers is most likely caused by the $(Mg,Fe)_2SiO_4$ β-to-γ phase transformation. We show that the formation of $CaSiO_3$ perovskite from garnet can cause the deeper discontinuity, and by determining the temperature dependence for this reaction we demonstrate that regional variations in splitting of the discontinuity arise from variability in the calcium concentration of the mantle rather than from temperature changes. This discontinuity therefore is sensitive to large-scale chemical heterogeneity. Its occurrence and variability yield regional information on the fertility of the mantle or the proportion of recycled oceanic crust.

Recent regional seismic observations have identified multiple discontinuities near the depth of the 520-km discontinuity in the transition zone (*1*–*4*). Beneath some regions, this discontinuity splits into two discontinuities, one at a depth of about 500 km and the other near 560 km (*1*). The depth of these two discontinuities varies, implying that they are marking phase transitions that are responding to variations in composition between regions of the mantle or to varying temperature. The wadsleyite-to-ringwoodite (β-γ) transition is often implicated as the cause of the 520-km discontinuity (*5*). However, the exsolution of $CaSiO_3$ perovskite from majoritic garnet that also occurs at a similar depth could cause the observed higher pressure split in the 520-km discontinuity (*6*). This reaction is complex because majoritic garnet is a multicomponent solid solution. Existing data (*7*–*10*) are not sufficiently consistent for modeling how the reaction varies with respect to pressure, temperature, and mantle composition. We studied the exsolution of Ca perovskite in high-pressure and -temperature experiments in order to ascertain the depth interval over which the reaction occurs. We also estimated the jump in density and sound velocity expected for this reaction and used these data to explain regional occurrences of single and split 520-km discontinuities.

At mid-transition-zone pressures (17 GPa), garnet will contain all of the Ca in most plausible mantle chemical compositions and will have a substantial majorite component (i.e., $Mg_4Si_4O_{12}$), which results from the substitution of Si and Mg into the Al site at high pressure (*11*, *12*). The proportions of Ca and Al in transition-zone garnets will vary strongly between different rock types, being low in rocks of peridotite composition but much higher in rocks that are remnants of subducted oceanic crust, that is, with the composition of midocean ridge basalt (MORB). With increasing pressure, Ca perovskite exsolves from garnet as the solubility of $CaSiO_3$ in garnet decreases. We measured this solubility in multianvil experiments between 15 and 24 GPa at 1400° and 1600°C and as a function of the garnet majorite content (i.e., Al/Si ratio). Ca-free glass compositions on the join $(Mg,Fe)_4Si_4O_{12}$–$(Mg,Fe)_3Al_2Si_3O_{12}$ were mixed with presynthesized $CaSiO_3$ wollastonite in a 1:2 weight ratio to produce starting materials for multianvil experiments. These samples were loaded into rhenium capsules that contained four sample chambers (Fig. 1). Three samples with varying Al/Si ratios were loaded into each experiment, plus a $(Mg,Fe)_2SiO_4$ sample to calibrate the pressure. During the experiment, the glass and $CaSiO_3$ compositions crystallize rapidly to form garnet and perovskite, respectively, and $CaSiO_3$ dissolves into the garnet (*13*). The diffusion into the garnet is slow, and experiments must be equilibrated for at least 24 hours in order to reach equilibrium. A B_2O_3 flux was also added to speed up the reaction. Some experiments were reversed by first synthesizing Ca-bearing garnets and measuring their compositions after $CaSiO_3$ had subsequently exsolved at a particular pressure and temperature. After the experiments had been quenched, recovered samples were analyzed with an electron microprobe. During the experiments, the $(Mg,Fe)_2SiO_4$ olivine pressure calibrant crystallized to form coexisting high-pressure phases. The pressure could be determined because the high-pressure Mg_2SiO_4-Fe_2SiO_4 phase diagram consists of a series of two-phase divariant loops where the Fe/(Fe+Mg) ratios of coexisting phases are very sensitive to pressure. In this way, we calibrated accurately the pressure of Ca-perovksite formation relative to the pressure of phase transformations in the Mg_2SiO_4-Fe_2SiO_4 system (*13*–*15*).

Our data (Fig. 2) show that the solubility of $CaSiO_3$ in garnet in equilibrium with Ca perovskite decreases strongly with pressure, but it increases with the garnet Al/Si ratio at a given pressure, which can be seen by comparing results from the different starting compositions. At lower temperatures (1400°C), $CaSiO_3$ solubility in gar-

---

Bayerisches Geoinstitut, University of Bayreuth, D-95444 Bayreuth, Germany.

*To whom correspondence should be addressed. E-mail: ashima.saikia@uni-bayreuth.de